Dissipation and its consequences in the scaling exponents for a family of two-dimensional mappings

2012 J. Phys. A: Math. Theor. 45 165101

(http://iopscience.iop.org/1751-8121/45/16/165101)

IOP Publishing Journal of Physics A: Mathematical and Theoretical

J. Phys. A: Math. Theor. **45** (2012) 165101 (11pp) doi:10.1088/1751-8113/45/16/165101

Dissipation and its consequences in the scaling exponents for a family of two-dimensional mappings

Juliano A de Oliveira and Edson D Leonel

Departamento de Estatística, Matemática Aplicada e Computação, UNESP—Univ Estadual Paulista, Av. 24A, 1515 Bela Vista, CEP 13506-900, Rio Claro, SP, Brazil

E-mail: julianoantonio@gmail.com and edleonel@rc.unesp.br

Received 12 December 2011, in final form 6 March 2012
Published 10 April 2012
Online at stacks.iop.org/JPhysA/45/165101

Abstract

The effects and consequences of dissipation in the scaling exponents describing the behaviour of average properties over the chaotic dynamics for a family of two-dimensional mappings are studied. The mapping is parametrized by an exponent γ in one of the dynamical variables and by a parameter $\delta \in [0, 1]$, which denotes the amount of the dissipation. The Lyapunov exponents are obtained for different values of γ and δ in the range $0 < \delta < 1$. The behaviour of the approaching orbits to the chaotic attractors is described analytically to be of exponential type. The deviation around the average action for chaotic orbits was described by a single set of scaling exponents obtained for different γ leading the model to fall into the same universality class as that of the dissipative bouncer model.

PACS numbers: 05.45.Ac, 05.45.Pq, 05.45.Tp

(Some figures may appear in colour only in the online journal)

1. Introduction

The study of dynamical properties of two-dimensional nonlinear mappings is a topic that draws attention in various areas of physics, ranging from general systems [1, 2], periodically corrugate waveguides [3–5], channel flows [6, 7], billiards [8], Fermi acceleration [9, 10], study of magnetic field lines in toroidal plasma devices with reversed shear (like tokamaks) [11, 12], suppression and production of Fermi acceleration [13] and many others.

The mappings may have different control parameters controlling the dynamics and phase regimes including a transition from integrability to non-integrability. In the conservative case, certain ranges of control parameters produce a mixed phase space showing chaotic seas surrounding periodic islands and invariant spanning curves [1]. The introduction of dissipation generally made by a damping coefficient destroys the conservative structure, and elliptic fixed

points may bifurcate into sinks leading to a permanent trapping of the dynamics to a steady state. Chaotic seas may give rise to chaotic attractors. Invariant spanning curves are also destroyed. Hence, it is possible to observe a variety of different behaviours when the damping is varied. Examples of dissipative dynamical systems related to a variety of fields of physics that are treated by the use of discrete mappings can be found in [14–25] and references therein.

In this paper, we consider a family of dissipative two-dimensional nonlinear mappings parametrized by an exponent γ in one of the dynamical variables. There is also a control parameter ϵ controlling the nonlinearity of the mapping. For $\epsilon = 0$ and considering the conservative case, the mapping is integrable; therefore, we consider $\epsilon \neq 0$. We are seeking to understand and describe the influences and consequences of the dissipation in average observables obtained for chaotic orbits. The dissipation is introduced by the use of a control parameter δ such that, for $\delta = 1$, the conservative system is recovered; hence, we consider the case of $\delta < 1$. We have shown that given an initially large action, the convergence to the chaotic attractor was proved analytically to be of exponential type. Moreover, some scaling properties along the chaotic attractor were considered and scaling exponents describing the average of the mean action are numerically obtained. The knowledge of such exponents allows us to define and compare universality classes for two-dimensional mappings [26]. Indeed for the non-dissipative case and considering the angle as a diverging function in the limit of vanishing action, the phase space is mixed containing periodic islands, chaotic seas and invariant spanning curves. The first of these can be estimated via a connection with the standard mapping [27], where it is supposed that the phase space experiences a transition from local to globally chaotic dynamics (see [1] for specific discussions and [27] for recent results). The behaviour for the average action of the chaotic sea is described by the same law that describes the position of the first invariant spanning curve in the phase space and scales with a function of γ. Such a scale produces a family of different exponents characterizing the average action, which is described via a homogeneous function. Therefore, the different exponents define different universality classes. The main result obtained for the dissipative case and in contrast to what is observed for the corresponding non-dissipative case of the mapping (see [26]) is that the dissipation leads the average action to be characterized by a single set of critical exponents even when the parameter γ is varied. Therefore, dissipation destroys the different universality classes observed in the non-dissipative case leading the dynamics to fall into a single set of critical exponents. This paper then discusses the results for the critical exponents in the dissipative dynamics. The procedure used in this paper to obtain the critical exponents consists in investigating the behaviour of the average action in the chaotic attractor and hence its deviation around the average value. In the absence of dissipation and for the control parameters considered, the action presents an unlimited diffusion. However, the introduction of dissipation causes a shrink in the phase space and localized attractors appear. Such attractors have properties that depend on the control parameters. Our contribution to this study is to describe some of these properties using the formalism of scaling. In fairness, we show that the fine structure observed in the non-dissipative case with the occurrence of a continuous set of critical exponents [26, 27] as a function of γ is entirely destroyed in the dissipative case. The latter produces a single set of critical exponents.

The paper is organized as follows. In section 2, we present the model and discuss the variables and control parameters used. Section 3 is devoted to the analytical approach for the convergence of the orbits towards the chaotic attractor and the discussion of the Lyapunov exponents. Section 4 addresses the scaling properties for the chaotic attractors. Finally, in section 5, we present our concluding remarks.

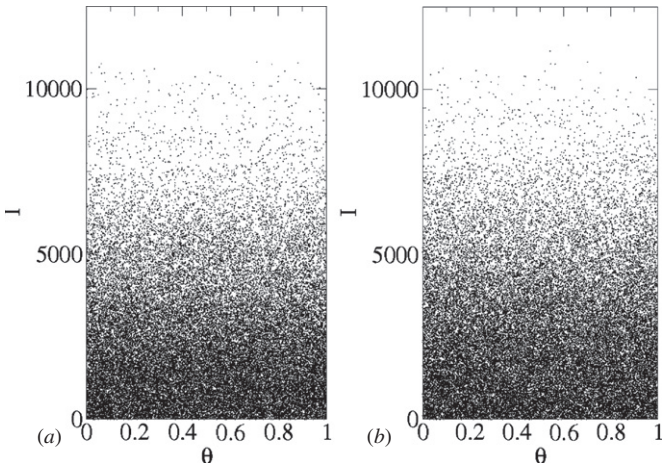

Figure 1. Chaotic attractors generated for the mapping (1) for the control parameters, $\epsilon = 100$, $\delta = 0.999$ in (a) $\gamma = 3/5$ and (b) $\gamma = 2$. We used a grid of 10×10 $(= 100)$ different initial conditions uniformly distributed in the window $I_0 \in [0.01, 1]$ and $\theta_0 \in [0.1, 1]$. Each initial condition was evolved up to 5×10^3 iterations.

2. The model and the map

The dynamical system considered in this paper takes into account the introduction of dissipation in a family of two-dimensional Hamiltonian mappings [1]. The mappings are defined as

$$T : \begin{cases} I_{n+1} = |\delta I_n - (1+\delta)\epsilon \sin(2\pi\theta_n)| \\ \theta_{n+1} = \left[\theta_n + I_{n+1}^{\gamma}\right] \bmod 1, \end{cases} \tag{1}$$

where the parameter ϵ controls the nonlinearity, δ is the parameter controlling the amount of dissipation and γ is a free parameter. The variable θ is indeed modulated 1. The determinant of the Jacobian matrix of the mapping (1) is $\mathrm{Det\,J} = \delta \mathrm{sign}\,[\delta I_n - (1+\delta)\epsilon \sin(2\pi\theta_n)]$, where the function $\mathrm{sign}(u) = 1$ if $u > 0$ and $\mathrm{sign}(u) = -1$ if $u < 0$. For $\delta = 1$, the conservative case is recovered. Moreover, different mappings are obtained according to the values of γ. For the case of $\delta \neq 1$ and $\gamma = 1$, and considering the transformations $I_{n+1} \to V_n$, $2\pi\theta \to \phi$ and $n \to n+1$, one can recover the dissipative bouncer model [28, 29]. Considering $\gamma = -1$, $\delta = 1$ and taking into account the following transformations $I \to V$ and $2\pi\theta \to \phi$, one recovers the conservative Fermi–Ulam accelerator model [10]. For the case of $\delta = 1$, $\gamma = -1$, $2\pi\theta \to X$ and $I \to \gamma$, where γ in this transformation represents the angular coordinate instead of the control parameter, one has the periodically corrugated waveguide [3]. On the other hand, for the case of $\delta = 1$ and $\gamma = -1/2$, one endeavours to obtain and describe the dynamical properties of a particle in a wave packet [30].

In this paper, we consider the dynamics given by mapping (1). The more natural observable to look at is the average action $\bar{I}$, and hence, the deviation of average $\bar{I}$ for chaotic orbits for different values of γ, which we consider in this paper as non-negative. Following [26], different universality classes were obtained for the conservative case considering different values of γ. As we will see, the dissipation destroys such universality classes leading the dynamics to be characterized by a single set of scaling exponents instead of several sets as observed in the non-dissipative case. The time evolution of different initial conditions is shown in figure 1 for the control parameters $\epsilon = 100$, $\delta = 0.999$ in (a) $\gamma = 3/5$ and (b) $\gamma = 2$. As one can

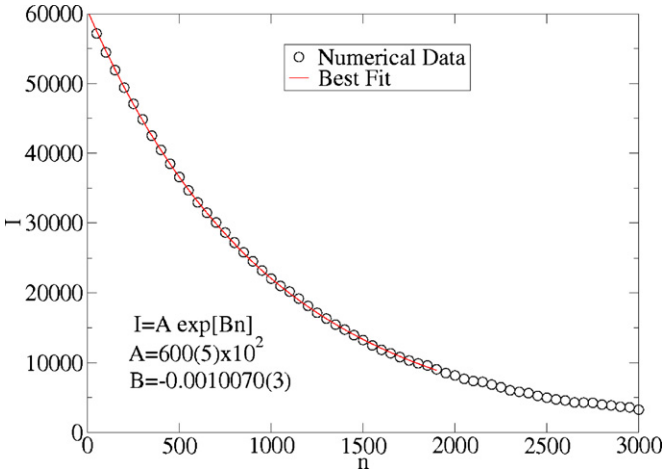

Figure 2. Behaviour of I versus n using $\epsilon = 10$, $\delta = 0.999$, $I_0 = 60\,000$, $\theta_0 = 0.01$ and $\gamma = 2$.

note, the different values of γ do not produce substantial changes in the chaotic attractors. We used a grid of 10×10 ($= 100$) different initial conditions uniformly distributed in the window $I_0 \in [0.01, 1]$ and $\theta_0 \in [0.1, 1]$. Each initial condition was evolved up to 5×10^3 iterations.

3. Approaching orbits to chaotic attractors and Lyapunov exponents

Let us discuss in this section an analytical argument for approaching orbits to the chaotic attractors. To do so, as an initial condition we consider a large value of I_0. Given the system is dissipative and therefore shrinks in area in the phase space, it is expected that a large initial action I_0 will lead the dynamics to low values of I as time goes on. We then want to describe this decay of the action as a function of n. To do so, we iterate the second equation of the mapping (1) and obtain

$$\begin{aligned} I_1 &= |\delta I_0 - (1+\delta)\epsilon \sin(2\pi\theta_0)|, \\ I_2 &= |\delta^2 I_0 - (1+\delta)\epsilon\,[\delta \sin(2\pi\theta_0) + \sin(2\pi\theta_1)]\,|, \\ I_3 &= |\delta^3 I_0 - (1+\delta)\epsilon[\delta^2 \sin(2\pi\theta_0) + \delta \sin(2\pi\theta_1) + \sin(2\pi\theta_2)]|. \end{aligned} \tag{2}$$

A general expression can be written as

$$I_n = \delta^n I_0 - (1+\delta)\,\epsilon \sum_{i=1}^{n} \delta^{n-i} \sin(2\pi\theta_{i-1}). \tag{3}$$

Given the periodicity of the sine function, the second term in the above equation after the equality can be neglected as it contributes very little to the average, mainly producing small oscillations around the average decay. This procedure also let us to disregard the behaviour of θ given by the second equation of mapping (1). The first term on the right-hand side marks clearly an exponential decay. Figure 2 shows the behaviour of I given by mapping (1) as a function of n for the control parameters $\epsilon = 10$, $\delta = 0.999$, $I_0 = 60\,000$, $\theta_0 = 0.01$ and $\gamma = 2$. One sees that an exponential decay of I with n is clearly observed. We show in figure 2 that an exponential fit of the type $I = A\,\mathrm{e}^{B\theta}$ gives $A = 600(5) \times 10^2$ and $B = -0.001\,0070(3)$.

The chaotic orbits were characterized using the Lyapunov exponents. The basic principle to obtain the Lyapunov exponents consists in verifying if two neighbouring orbits diverge

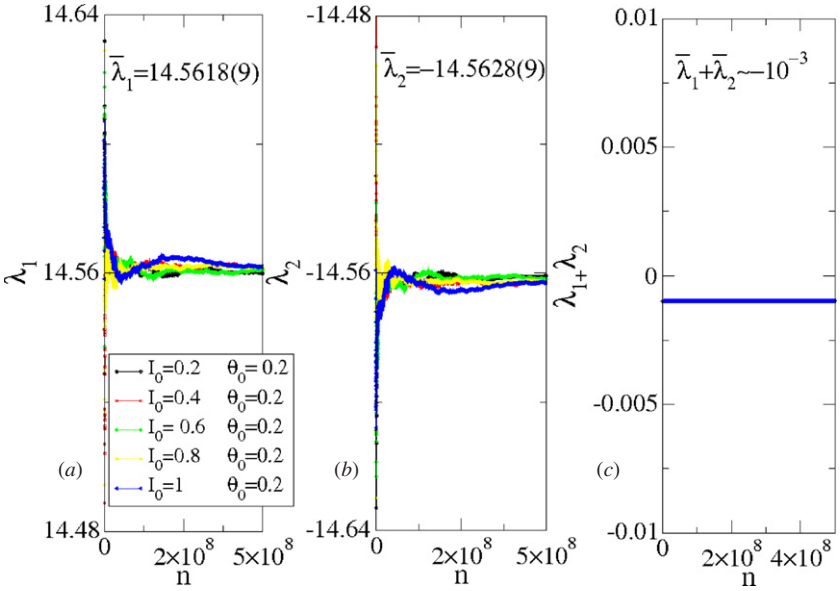

Figure 3. Plots of λ versus n for the control parameters $\epsilon = 100$, $\delta = 0.999$ and $\gamma = 2$: (*a*) positive Lyapunov exponent, (*b*) negative Lyapunov exponent and (*c*) summation of (*a*) and (*b*).

exponentially from each other as time goes on. If the orbits remain close or approach each other during the long time, their dynamics is said to be regular. This implies that the Lyapunov exponent is negative, $\lambda < 0$ or null $\lambda = 0$. If the orbits diverge exponentially in time, the dynamics has a positive Lyapunov exponent $\lambda > 0$. In conservative systems, the sum of Lyapunov exponents is equal to zero because of the area preservation in the phase space. When dissipation is introduced in the system, area contraction is in course and the sum of both Lyapunov exponents is no longer zero. The Lyapunov exponents are defined as in [31] (see also [32] for a recent review on the topic):

$$\lambda_j = \lim_{n\to\infty} \frac{1}{n} \ln \left|\Lambda_j^{(n)}\right|, \qquad j = 1, 2, \tag{4}$$

where $\Lambda_j^{(n)}$ are the eigenvalues of the matrix $M = \Pi_{i=1}^{n} J_i(\theta, I)$, where J_i is the Jacobian matrix of the mapping evaluated along the orbit.

In figure 3, the behaviour of the Lyapunov exponents averaged along the chaotic attractor for mapping (1) is shown. Figures 3(*a*) and (*b*) show the behaviour of the (positive/negative) Lyapunov exponent as a function of n, while figure 3(*c*) shows their summation. The parameters $\epsilon = 100$, $\delta = 0.999$ and $\gamma = 2$ and five different initial conditions as labelled in the figure were used. We obtained a convergence for the positive Lyapunov exponent as $\bar{\lambda}_1 = 14.5618(9)$ and $\bar{\lambda}_2 = -14.5628(9)$ for the negative. The error 0.0009 in both cases corresponds to a standard deviation of the five samples. The summation of $\bar{\lambda}_1 + \bar{\lambda}_2$ is of the order of -10^{-3}, as shown in figure 3(*c*), which is of the same magnitude as that of $(1 - \delta)$.

We now discuss the behaviour of the Lyapunov exponents as a function of the parameters ϵ, δ and γ. In figures 4(*a*) and (*d*), the behaviour of $\bar{\lambda}$ versus $(1-\delta)$ for fixed $\epsilon = 100$ and $\gamma = 2$ while $\delta \in [0.99, 0.999\,99]$ is shown. For this case, the negative Lyapunov exponent shown in figure 4(*a*) grows logarithmically, while the positive Lyapunov exponent in figure 4(*d*) decreases logarithmically with $(1 - \delta)$. A fitting for the negative Lyapunov exponent furnishes $\bar{\lambda}_2 = -11.114(2) + 0.4989(2)\ln(1 - \delta)$, while for the positive Lyapunov exponent it gives

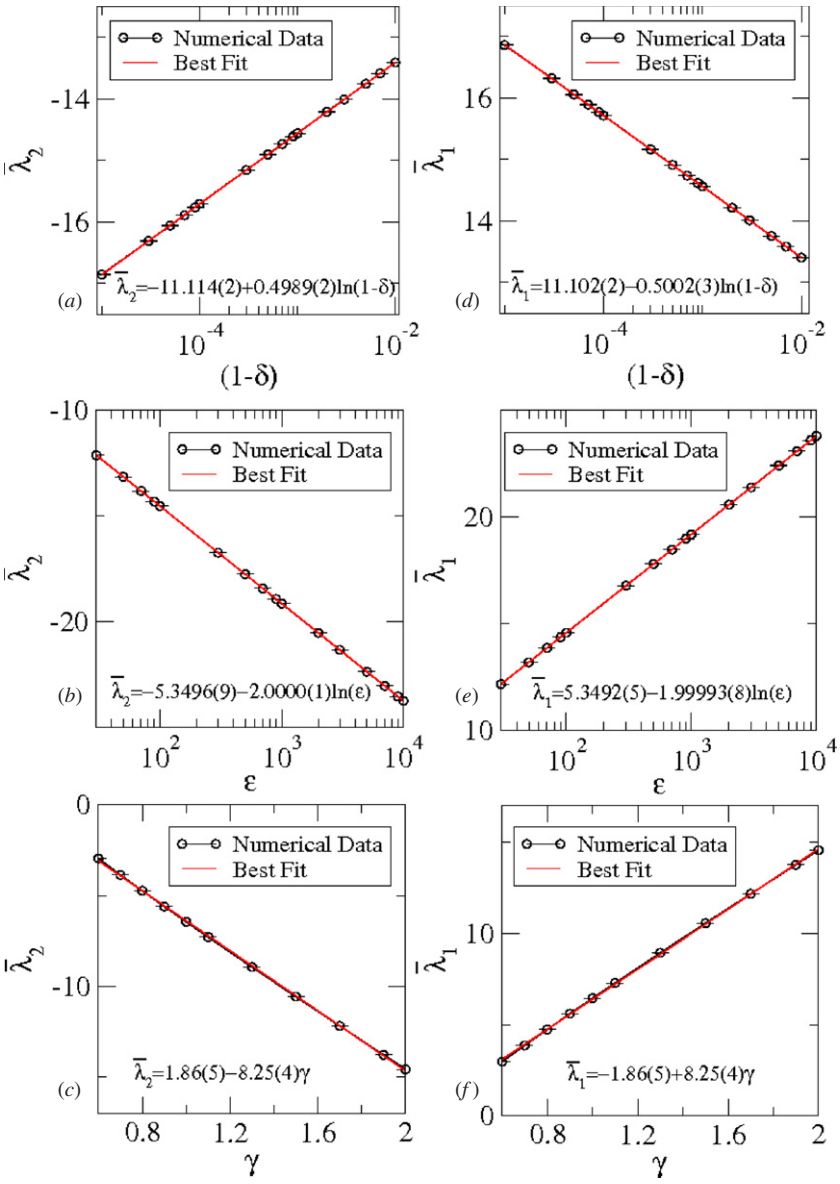

Figure 4. Plots of the negative (first column) and positive (second column) Lyapunov exponent as function of: (*a, d*) $(1-\delta)$; (*b, e*) ϵ and; (*c, f*) γ.

us $\bar{\lambda}_1 = 11.102(2) - 0.5002(3)\ln(1-\delta)$. A logarithmic behaviour was also observed in figures 4(*b*) and (*e*) for the case of $\bar{\lambda}$ versus ϵ for a fixed $\delta = 0.999$, $\gamma = 2$ and a large range of $\epsilon \in [10, 10^3]$. For this case, we see that the negative Lyapunov exponent in figure 4(*b*) decreases logarithmically with ϵ. Again a fitting gives us $\bar{\lambda}_2 = -5.3496(9) + 2.0000(1)\ln(\epsilon)$. Figure 4(*e*) shows that the positive Lyapunov exponent grows logarithmically with ϵ as $\bar{\lambda}_1 = 5.3492(5) + 1.99\,993(8)\ln(\epsilon)$. The variation of the control parameter γ produces a change in the Lyapunov exponent, as shown in figures 4(*c*) and (*f*) for $\bar{\lambda}$ versus γ. The control

parameters considered in both figures were $\epsilon = 100$ and $\delta = 0.999$, while $\gamma \in [3/5, 2]$. We observe in figure 4(*c*) that the negative Lyapunov exponent decreases linearly with the control parameter γ. A fitting furnishes $\bar{\lambda}_2 = 1.86(5) - 8.25(4)\gamma$, while figure 4(*f*) shows a linear growth for the positive Lyapunov exponent given as $\bar{\lambda}_1 = -1.86(5) + 8.25(4)\gamma$.

4. Scaling properties

In the conservative case, the presence of the invariant spanning curves limit the size of the chaotic sea at low action. It was shown previously [3, 10, 26, 27, 30] that scaling properties are observed in the chaotic sea and that they depend on the position of the first invariant spanning curve [27]. The exponents describing the laws of the average quantities in the chaotic sea depend on the exponent γ. Therefore, as γ changes, the exponents of the laws vary too, following the law that describes the position of the first invariant spanning curve. For the dissipative case, the invariant spanning curves are destroyed and chaotic attractors may appear, for specific ranges of control parameters, replacing the chaotic seas. Scaling properties for the dissipative case were also considered [28, 29] and universality classes were obtained. Therefore, in this section, we discuss the deviation of the average action for chaotic attractors denoted as ω. Our main goal is to compare the exponents describing the laws of the average quantities in the chaotic attractors with those obtained for both the conservative [26, 27] and the dissipative cases [28, 29]. The observable ω is defined as

$$\omega(n, \epsilon, \delta) = \frac{1}{B}\sum_{i=1}^{B}\sqrt{\overline{I_i^2}(n, \epsilon, \delta) - \overline{I_i}^2(n, \epsilon, \delta)}, \tag{5}$$

where B corresponds to an ensemble of different initial conditions $\theta_i \in (0, 1)$ randomly chosen for a fixed $I_0 = 10^{-3}\epsilon$ and $\bar{I}_i$ is given by

$$\overline{I}_i(n, \epsilon, \delta) = \frac{1}{n}\sum_{j=1}^{n} I_{j,i}. \tag{6}$$

Figure 5 shows the behaviour of ω versus n for the exponent $\gamma = 2$ and different control parameters (as labelled in the figure). Similar results were observed for other values of γ too.

Let us now discuss the behaviour observed in figure 5. We see that the curves start growing for small n and after reaching a crossover number n_x, they bend towards a regime of convergence. Based on the behaviour shown in figure 5, we suppose the following.

(i) For $n \ll n_x$, ω grows according to a power law of the type

$$\omega \propto (n\epsilon^2)^{\beta}, \tag{7}$$

where β is an exponent.

(ii) For large n, say $n \gg n_x$, the behaviour of ω is

$$\omega_{\text{sat}} \propto (1 - \delta)^{\alpha_1}\epsilon^{\alpha_2}, \tag{8}$$

where α_1 and α_2 are the critical exponents;

(iii) The crossover n_x, which characterizes the transition of the growing regime for the saturation, is

$$n_x \propto (1 - \delta)^{z_1}\epsilon^{z_2}, \tag{9}$$

where z_1 and z_2 are the dynamical exponents.

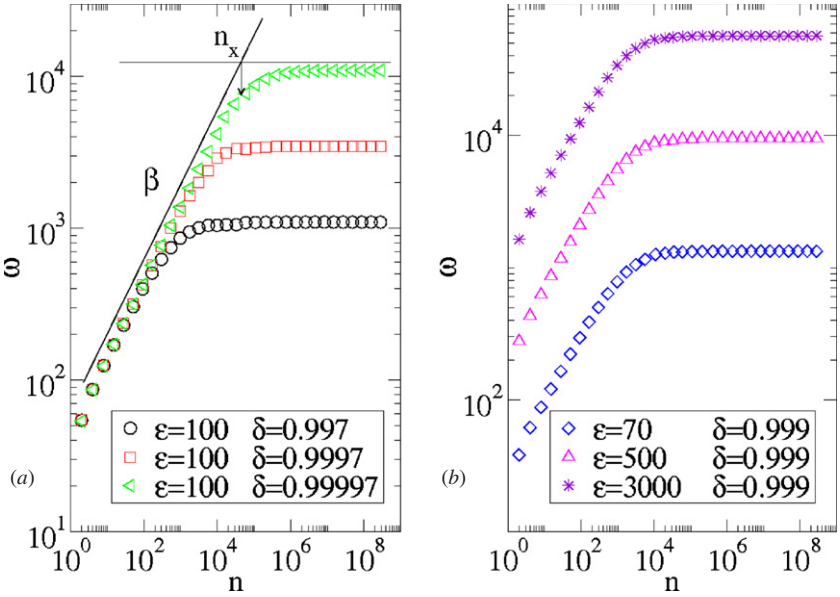

Figure 5. Plots of different curves of ω as a function of n for the control parameter $\gamma = 2$ and different values of (*a*) δ and (*b*) ϵ. We considered an ensemble of $B = 5000$ different initial conditions.

The critical exponents α_1, α_2, z_1 and z_2 can be obtained from numerical simulations. First, fitting the initial regime of growth over many different simulations, we obtain that $\beta \cong 0.5$. The other exponents are obtained from specific plots. In figures 6(*a*) and (*b*), plots of n_x versus $(1-\delta)$ and ω_{sat} versus $(1-\delta)$, respectively, for the case of $\epsilon = 100$ are shown. On the other hand, in figures 6(*c*) and (*d*), plots of n_x versus ϵ and ω_{sat} versus ϵ for $\delta = 0.999$ are shown. All the results shown in figure 6 were obtained for a fixed $\gamma = 2$ and using long simulations of 5×10^8 iterations. The ensemble average used was $B = 5 \times 10^3$. Power-law fittings for the curves plotted in figure 6 furnish (*a*) $z_1 = -0.990(5)$ and (*b*) $\alpha_1 = -0.502(1)$, and (*c*) $z_2 = 2.006(7)$ and (*d*) $\alpha_2 = 0.999\,99(4)$.

Indeed the scaling hypotheses shown in equations (7)–(9) allow us to formally describe the behaviour of ω as a homogeneous and generalized function. If a similar procedure is made as discussed in [29] and after rescaling the axis of figure 5 as $\omega \to \omega/[(1-\delta)^{\alpha_1}\epsilon^{\alpha_2}]$ and the horizontal axis as $n \to n\epsilon^2/[(1-\delta)^{z_1}\epsilon^{z_2}]$, we show in figure 7 that all the curves shown in figure 5 overlap each other onto a single and hence universal plot. Therefore, this confirms that the behaviour of ω is scaling invariant with respect to the control parameters as well as n.

The curves of ω were obtained for a fixed $\gamma = 2$. The procedure works well for other values of γ in the range $\gamma \in [3/5, 2]$. In tables 1 and 2, the scaling exponents found via numerical simulations for different values of γ are given. The scaling exponents given in table 1 were obtained for a fixed control parameter $\epsilon = 100$ and different values of δ. Keeping fixed the control parameter $\delta = 0.999$ and considering different values of ϵ, the critical exponents are given in table 2.

Let us now discuss the consequences of the dissipation in the critical exponents. As was discussed recently for the conservative case [26], the critical exponents obtained there are different for different values of γ. The variation of γ leads to several universality classes characterized by different critical exponents. Later on we explained (see [27]) in terms of a

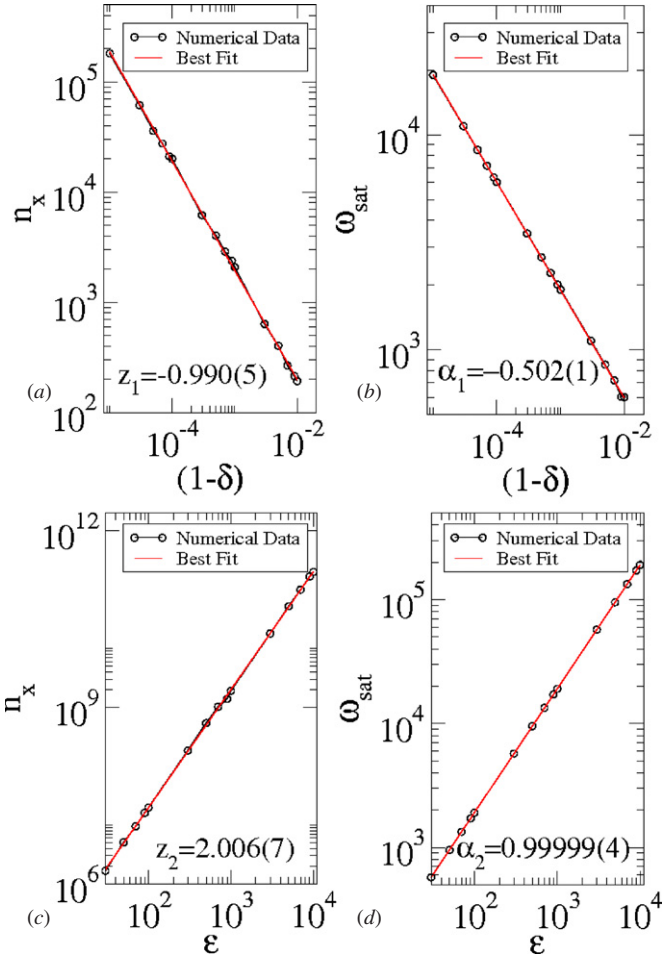

Figure 6. Plots of n_x and ω_{sat} for a fixed $\gamma = 2$ as a function of (a, b) $(1 - \delta)$ for $\epsilon = 100$ and (c, d) ϵ for $\delta = 0.999$.

Table 1. Scaling exponents obtained for $\epsilon = 100$ and $\delta \in [0.99, 0.999\,99]$ for the mapping (1).

γ	β	α_1	z_1
3/5	0.496(6)	−0.508(1)	−1.028(4)
3/4	0.496(4)	−0.5005(3)	−0.989(4)
4/5	0.496(5)	−0.5010(2)	−0.989(4)
1	0.494(5)	−0.496(2)	−0.988(6)
2	0.496(5)	−0.502(1)	−0.990(5)

robust approach that the critical exponents are strongly dependent on the position of the first invariant spanning curve for the conservative case. In this paper, the invariant spanning curves are destroyed and therefore are not observed because of the dissipative term. Moreover, after a close look at both tables 1 and 2 we see no significant differences of the scaling exponents for several variations of the exponent γ. Moreover, we conclude that the fine hierarchy of the different universality classes observed for the non-dissipative case of equation (1) is destroyed

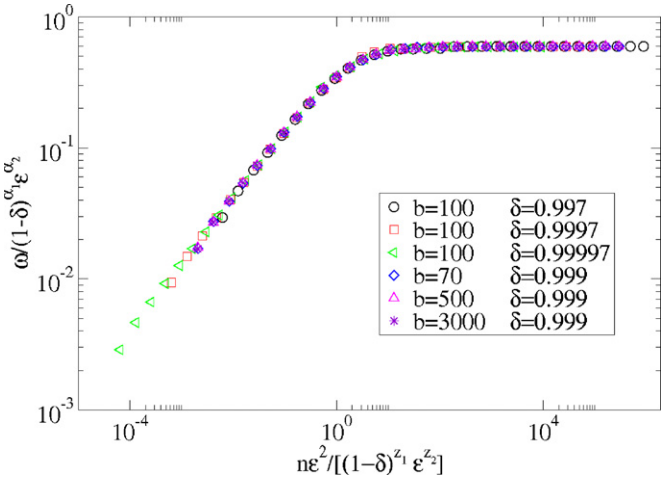

Figure 7. Overlap of different curves of ω onto a single plot. The parameters used are the same as those shown in figure 5.

Table 2. Scaling exponents obtained for the range $\epsilon \in [10, 10^3]$ and $\delta = 0.999$ for the mapping (1).

γ	β	α_2	z_2
3/5	0.489(5)	0.9975(7)	1.987(9)
3/4	0.492(5)	0.9970(9)	1.977(4)
4/5	0.493(3)	0.9996(1)	1.995(3)
1	0.494(4)	1.0008(4)	1.997(5)
2	0.491(5)	0.999 99(4)	2.006(7)

by the dissipative term leading the dynamics to be characterized by a single set of critical exponents. The exponents obtained are independent of γ, and the dissipative mapping (1) leads the dynamics to fall into the same universality class as that of the dissipative bouncer model [28, 29].

5. Conclusion

We have studied the effects of dissipation in a family of two-dimensional mappings parametrized by an exponent γ in one of the dynamical variables. We have shown that the dissipation creates chaotic attractors and proved that the convergence to them coming from high action is of exponential type. The Lyapunov exponents were obtained as a function of the control parameters and fitted as logarithmically dependent on the parameter $(1 - \delta)$ and ϵ and linearly as a function of γ. Finally, a single set of scaling exponents was obtained for different values of the control parameter γ leading us to conclude that map (1) falls into the same universality class of the dissipative bouncer model [28, 29]. Therefore, we conclude that the fine structure observed in the phase space for the conservative case is destroyed in the presence of dissipation. The average action and hence its deviation around the average value lead us to observe a single set of critical exponents.

Acknowledgments

JAO thanks CNPq, Pró-reitoria de pesquisa da UNESP and CAPES. EDL kindly acknowledges the financial support from CNPq, FAPESP and FUNDUNESP, Brazilian agencies. JAO acknowledges Diogo R da Costa and André L P Livorati for discussions. This research was supported by resources supplied by the Center for Scientific Computing (NCC/GridUNESP) of the São Paulo State University (UNESP).

References

[1] Lichtenberg A J and Lieberman M A 1992 *Regular and Chaotic Dynamics (Applied Mathematical Sciences* vol 38*)* (New York: Springer)
[2] Zaslavsky G M 1998 *Physics of Chaos in Hamiltonian Systems* (London: Imperial College Press)
[3] Leonel E D 2007 *Phys. Rev. Lett.* **98** 114102
[4] Virovlyansky A L and Zaslavsky G M 2000 *Chaos* **10** 211
[5] Smirnov I P, Virovlyansky A L and Zaslavsky G M 2001 *Phys. Rev.* E **64** 036221
[6] Luna-Acosta G A, Méndez-Bermudéz J A, Seba P and Pichugin K N 2002 *Phys. Rev.* E **65** 046605
[7] Zaslavsky G M 2002 *Phys. Rep.* **371** 461
[8] Berry M V 1981 *Eur. J. Phys.* **2** 91
[9] Karlis A K, Papachristou P K, Diakonos F K, Constantoudis V and Schmelcher P 2006 *Phys. Rev. Lett.* **97** 194102
[10] Leonel E D, McClintock P V E and da Silva J K L 2004 *Phys. Rev. Lett.* **93** 014101
[11] Howard J E, Lichtenberg A J, Lieberman M A and Cohen R H 1986 *Physica* D **20** 259
[12] Luna-Acosta G A, Na K and Reichl L E 1996 *Phys. Rev.* E **53** 3271
[13] Ladeira D G and Leonel E D 2010 *Phys. Rev.* E **81** 036216
[14] Lieberman M A and Tsang K Y 1985 *Phys. Rev. Lett.* **55** 908
[15] Luck J M and Mehta A 1993 *Phys. Rev.* E **48** 3988
[16] Tavares D F and Leonel E D 2008 *Braz. J. Phys.* **38** 58
[17] Tsang K Y and Lieberman M A 1984 *Physica* D **11** 147
[18] Leonel E D and McClintock P V E 2006 *J. Phys. A: Math. Gen.* **39** 11399
[19] de Souza F A, Simões L E A, da Silva M R and Leonel E D 2009 *Math. Problems Eng.* **2009** 409857
[20] Castro Neto A H and Caldeira A O 1991 *Phys. Rev. Lett.* **67** 1960
[21] Rech P C, Beims M W and Gallas J A C 2005 *Phys. Rev.* E **71** 017202
[22] Seoane J M, Sanjuan M A F and Lai Y-C 2007 *Phys. Rev.* E **76** 016208
[23] Rosa J and Beims M W 2008 *Phys. Rev.* E **78** 031126
[24] Manchein C and Beims M W 2009 *Math. Problems Eng.* **2009** 513023
[25] Carneiro M V, Barroso J J and Macau E E N 2009 *Math. Problems Eng.* **2009** 345947
[26] de Oliveira J A, Bizão R A and Leonel E D 2010 *Phys. Rev.* E **81** 046212
[27] Leonel E D, de Oliveira J A and Saif F 2011 *J. Phys. A: Math. Theor.* **44** 302001
[28] Leonel E D and Livorati A L P 2008 *Physica* A **387** 1155
[29] Livorati A L P, Ladeira D G and Leonel E D 2008 *Phys. Rev.* E **78** 056205
[30] Oliveira D F M, Robnik M and Leonel E D 2011 *Chaos Solitons Fractals* **44** 883
[31] Eckmann J P and Ruelle D 1985 *Rev. Mod. Phys.* **57** 617
[32] Skokos Ch 2010 *Lect. Notes Phys.* **790** 63